Astronomy & Astrophysics

Relationship between non-thermal electron energy spectra and *GOES* classes

R. Falewicz[1], P. Rudawy[1], and M. Siarkowski[2]

[1] Astronomical Institute, University of Wrocław, 51-622 Wrocław, ul. Kopernika 11, Poland
    e-mail: [falewicz;rudawy]@astro.uni.wroc.pl
[2] Space Research Centre, Polish Academy of Sciences, 51-622 Wrocław, ul. Kopernika 11, Poland
    e-mail: ms@cbk.pan.wroc.pl

ABSTRACT

Aims. We investigate influence of variations in the energy spectrum of non-thermal electrons on the resulting *GOES* classes of solar flares.
Methods. Twelve observed flares with various soft-to-hard X-ray emission ratios were modeled using different non-thermal electron energy distributions. Initial values of the flare physical parameters including geometrical properties were estimated using observations.
Results. We found that, for a fixed total energy of non-thermal electrons in a flare, the resulting *GOES* class of the flare can change significantly by varying the spectral index and low energy cut-off of the non-thermal electron distribution. Thus, the *GOES* class of a flare depends not only on the total non-thermal electrons energy but also on the electron beam parameters. For example, we were able to convert a M2.7 class solar flare into a merely C1.4 class one and a B8.1 class event into a C2.6 class flare. The results of our work also suggest that the level of correlation between the cumulative time integral of HXR and SXR fluxes can depend on the considered HXR energy range.

Key words. Sun: chromosphere – Sun: corona – Sun: flares – Sun: magnetic fields – Sun: X-rays, gamma rays

1. Introduction

The source and acceleration mechanisms of particles in solar flares remain far from being understood. During the flare impulsive phase, it is commonly accepted that, non-thermal electron beams are accelerated in the solar corona and move along magnetic field lines to the chromosphere, where they deposit their energy. Here, most non-thermal electrons lose their energy in Coulomb collisions, while a tiny part of the electron energy is converted into hard X-rays (HXR) by bremsstrahlung. The heated chromospheric plasma evaporates and radiates over a wide spectral range from hard X-rays or gamma rays to radio emission. Hard and soft X-ray fluxes emitted by solar flares are generally related, in a way first described by Neupert (1968), who found that the time derivative of the soft X-ray flux approximately matches the microwave flux during the flare impulsive burst. A similar effect was also observed for hard X-ray emission (Dennis & Zarro 1993). Since hard X-ray and microwave emissions is produced by non-thermal electrons and soft X-rays are generated by thermal emission from hot plasma, the Neupert effect suggests that non-thermal electrons are directly produce by plasma heating. Lin et al. (1984) were the first to observe hard X-ray emission above 25 keV from microflares using balloon-borne observations. Later studies using RHESSI observations (Qiu et al. 2004; Battaglia et al. 2005; Hannah et al. 2008) show that time, spatial, and spectral characteristics of microflares are similar to those of large flares. However, there is no universal, unambiguous correlation between the released total energy of the flare and the observed HXR radiation.

Many flares exhibit low SXR emission (as indicated by their GOES emission), but strong, HXR emission above 30 keV (McDonald et al. 1999; Gburek & Siarkowski 2002;

Qiu et al. 2004; Siarkowski et al. 2006). These events are commonly called "non-correlated" flares. Analytical estimations by McDonald et al. (1999) demonstrated that, in these flares, only a small part of the total energy carried by the non-thermal electrons is transferred to the ambient material during the chromospheric evaporation process. Even so, analysis of the HXR emission of these flares allows one to estimate the energy flux of non-thermal electrons and numerically simulate the energy losses and hydrodynamic effects of the chromospheric evaporation, thus allowing investigations of the energy budgets of the solar flares.

In this paper, we investigate the influence of non-thermal electron energy distribution on the resulting *GOES* classes of flares and energy used by chromospheric evaporation. Our goal is to separate the influence the spectral index (δ) and low energy cut-off (E_c) of the non-thermal electron distribution, taken to be a power law in energy, from the total energy of the electrons. To do this, we calculated a grid of 1D models to describe the time evolution of twelve observed solar flares. The models of each observed flare were calculated using identical total energies delivered by non-thermal electrons but with various appropriate combinations of δ and E_c. For each model, we calculated the resulting *GOES* 1–8 Å flux (i.e. *GOES* class of the event) as well as the evaporation energy.

In the following, we describe the observed flares (Sect. 2), the model calculation (Sect. 3), the results obtained (Sect. 4), and we present our discussion and conclusions in Sect. 5.

2. Observations

We selected 12 disk flares observed by the *Yohkoh* satellite, of simple single-loop X-ray structure and maximum hard X-ray
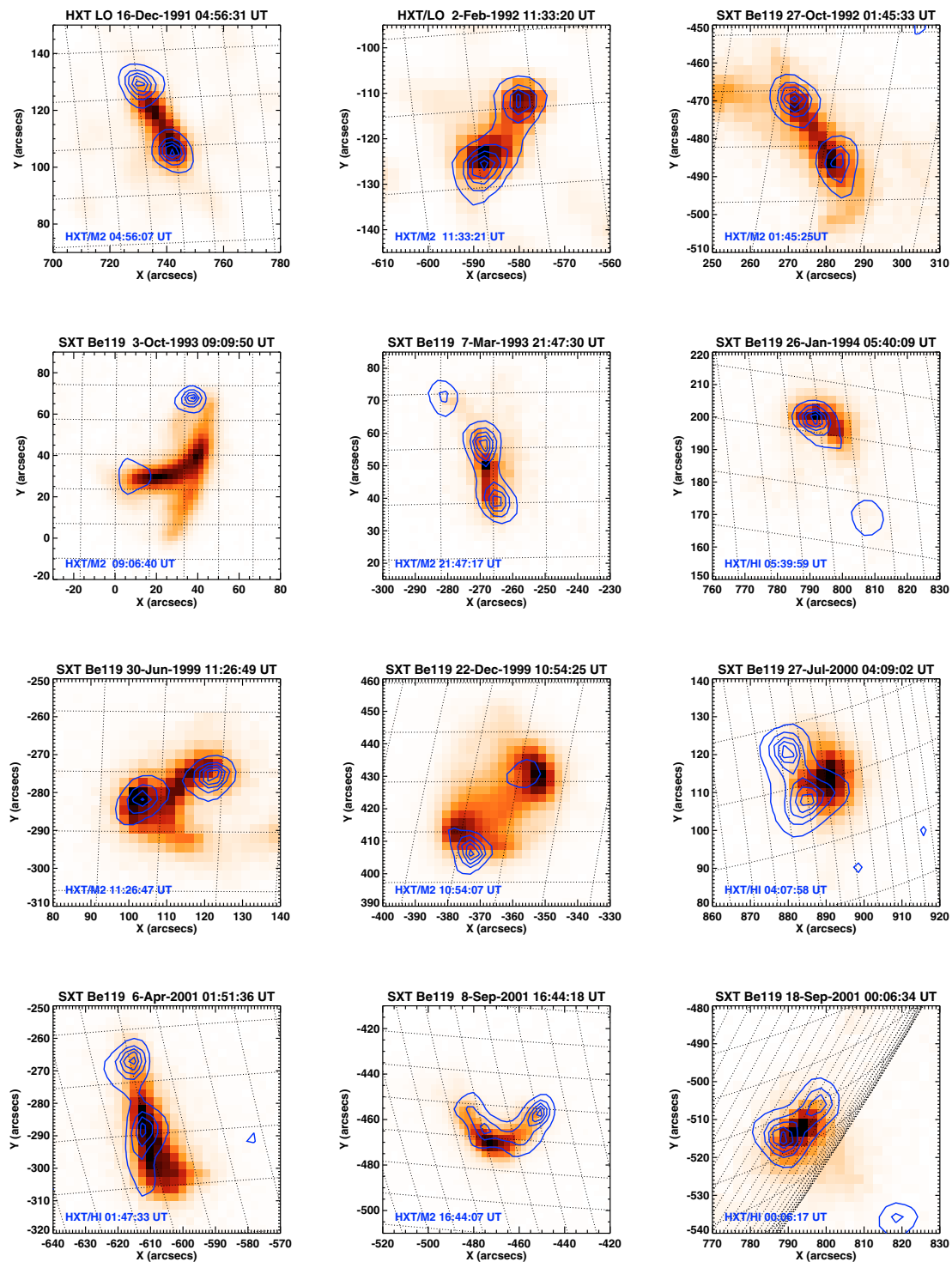
Fig. 1. Images of twelve analysed flares taken with the *Yohkoh* SXT or HXT/LO (gray scale images) and HXT/M2 or HXT/HI (contours) instruments.

flux not less than 10 cnts/s per subcollimator of the M2 channel (33–53 keV) of the HXT instrument (Kosugi et al. 1991). Details are given in Table 1. Five flares were analysed by McDonald et al. (1999) (four being correlated and one non-correlated), a further seven flares were taken from the HXT Flare Catalogue (Sato et al. 2006), four being correlated and three non-correlated. The correlated and non-correlated events are denoted in Table 1 with letters C and N, respectively.

The flares were also observed with the *Yohkoh* SXT grazing-incidence telescope (Tsuneta et al. 1991) and Bragg Crystal Spectrometer (*BCS*, Culhane et al. 1991), as well as the *GOES* X-ray photometers (1–8 Å and 0.5–4 Å bands). HXT images of the flares were reconstructed using a standard Pixon method (Metcalf et al. 1996) with variable accumulation times and an assumed threshold count rate of 200 counts in the M2 band (33–53 keV); these are shown in Fig. 1. SXR images (also shown) of

Table 1. Physical parameters of observed flares.

Event date	Time of maximum [UT]	GOES class	GOES incremental class	Type of flare	γ	a_0 [ph/cm^2/s/keV]	E_c [keV]	S [10^{17} cm^2]	L_0 [10^8 cm]
16-Dec.-91	04:58	M2.8	M2.7	C	3.6	7.6×10^6	25.8	3.9	15.4
02-Feb.-92	11:34	C5.5	C2.7	N	3.0	2.4×10^5	18.9	2.3	09.8
27-Oct.-92	01:47	M1.1	C9.5	C	4.5	2.8×10^7	25.2	2.3	11.6
03-Oct.-93	09:11	C1.0	B8.1	N	2.7	6.2×10^4	23.0	1.4	02.9
07-Mar.-93	21:48	C1.5	B9.2	N	3.0	4.8×10^4	24.0	2.3	12.6
26-Jan.-94	05:41	C1.4	C1.1	N	2.6	4.9×10^4	17.2	1.3	19.5
30-Jun.-99	11:30	M1.9	M1.8	C	3.4	1.0×10^6	25.8	1.8	11.5
22-Dec.-99	10:56	C6.4	C5.4	N	3.7	2.8×10^6	25.2	3.9	16.6
27-Jul.-00	04:10	M2.5	M2.4	C	3.2	4.8×10^5	19.8	2.3	08.7
06-Apr.-01	01:49	C7.8	C4.9	N	2.7	2.1×10^5	28.7	2.3	13.0
08-Sep.-01	16:45	C5.1	C3.2	N	2.9	2.0×10^5	29.6	2.3	17.0
18-Sep.-01	00:08	M1.5	M1.3	C	3.7	2.3×10^6	27.0	1.1	06.8

γ – photon spectral index; E_c – low energy cut-off; a_0 – scaling factor (flux at 1 keV); S and L_0 – cross-section and semi-length of the flaring loop; type of flare: *C* – correlated flare; *N* – non-correlated flare.

ten flares were taken with Be119/SXT, but for two flares, due to a lack of the SXT images, we present images taken with HXT in its L0 (14–23 keV) channel.

HXT spectra were analysed to obtain the photon spectral index (γ) at the flare peak time in the M2 channel, flux scaling factor (flux at 1 keV = a_0), and cut-off energy in the electron distribution (E_c). The SXT images allowed us to estimate the single loop semi-length (L_0) and cross-section (S). These are given in Table 1.

3. Methods of analysis

Solar flare hard X-ray emission $\gtrsim$10–20 keV is generally believed to be produced by bremsstrahlung emitted by non-thermal electrons. A power-law dependence of the emitted spectrum implies that the non-thermal electrons have a power law energy distribution (Brown 1971; Tandberg-Hanssen & Emslie 1988) and this in turn requires a low energy cut-off E_c to the electron spectrum to prevent an infinite total electron energy. A arbitrary value of E_c has been defined by numerous authors between 15 and 25 keV (see e.g., McDonald et al. 1999 and references therein). Thus, E_c occupies the energy range where thermal emission can dominate and so it is very difficult to determine its correct value from observations.

With the improved spectral resolution of the *RHESSI* instrument, the thermal and non-thermal spectral components can be more clearly separated. Direct inversion of photon spectra is now also possible to deduce the "mean electron flux distribution" (Brown et al. 2006). However, the problem of estimating E_c remains (e.g., Kontar et al. 2008). In the absence of *RHESSI* data for these flares, our approach has been to compare the *Yohkoh*/HXT observations of the 12 flares with the results of model calculations. We investigated the relation between the non-thermal electron spectra and the *GOES* class of the thermal flare, which is produced by evaporation processes, using the observed parameters of the 12 flares. Our calculations accounted for the observed energy distributions of the non-thermal electrons and time variations in the observed X-ray fluxes, dimensions of the flaring loops from SXR images, estimated main initial physical parameters of the thermal plasma (density, temperature), and energy gains and losses.

We analysed each flare in two steps: (a) we modeled the observed flare that most closely resembled the synthesised and observed *GOES* and BCS light curves (when available); (b) we investigated how the variations in the non-thermal electron energy spectra influence the synthesised *GOES* fluxes of a solar flare model.

The geometry of each flaring loop (volume (V), loop cross-section (S), and half-length (L_0)) were determined using images taken with SXT and HXT (see Table 1). The loop cross sections were estimated to be the areas within a level equal to 30% of the maximum flux in the HXT/M2 channel. Loop half-lengths L_0 were estimated from the distances between the centres of gravity of the HXT/M2 footpoints, assuming that the loop has a semi-circular shape. The volume of the loop V then equals $2L_0 \cdot S$. Temperatures (T_e) and emission measures (EM) were estimated using *GOES* 1–8 Å and 0.5–4 Å fluxes using the filter-ratio method proposed by Thomas et al. (1985). We used an updated version of this paper by White et al. (2005). A detailed description of this method is also given by Siarkowski et al. (2008). Mean electron densities (n_e) were estimated from emission measures (EM) and volumes ($V = 2L_0S$).

Assuming a power-law hard X-ray photon spectra $I(\epsilon) = a_0\epsilon^{-\gamma}$, we calculated time variations in the spectral indices (γ) and scaling factors a_0 (flux at 1 keV) for the impulsive phases of all 12 flares. Electron spectra of the form of $F = A E^{-\delta}$ can be calculated from power-law photon spectra using the thick target approximation (Tandberg-Hanssen & Emslie 1988):

$$A = a_0 \frac{4\pi R^2 C}{S \kappa_{BH}\bar{Z}^2} \frac{\gamma(\gamma-1)}{B(\gamma-1, \frac{1}{2})} \quad \text{and} \quad \delta = \gamma + 1, \tag{1}$$

where S is the loop cross-sectional area, R is the Earth-Sun distance (1 AU $\simeq 1.50 \times 10^{13}$ cm), κ_{BH} is the constant in the Bethe-Heitler cross-section (7.9×10^{-25} cm^2 keV), and $\bar{Z}^2$ is the abundance-weighted value of an atomic mass in the solar atmosphere, assumed to equal 1.4. The parameter C is defined to be $2\pi e^4\Lambda \approx 2.6 \times 10^{-18}$ cm^2 keV^2, where Λ is the Coulomb logarithm and $B(x, y)$ is the complete beta function. The total energies radiated in the SXR range were calculated by summing energies emitted by the flaring loop in all time-steps of the model over the duration of the flare impulsive phase, using for each time-step the measured temperature (T_e), electron density (n_e), and corresponding emission function.

The estimated total energy carried by the non-thermal electrons is very sensitive to the assumed low energy cut-off of the electron spectrum, E_c, because of the power-law nature of the
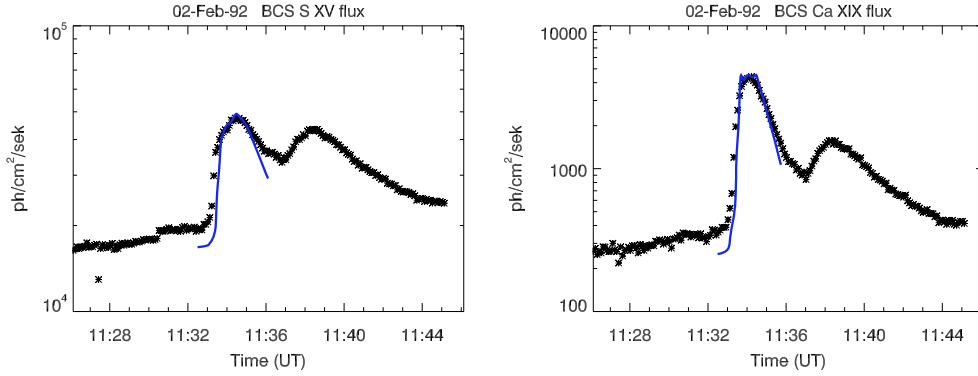
Fig. 2. Synthesised BCS CaXIX and BCS SXV fluxes (blue lines), and the observed fluxes (asterisks) of the C2.7 class solar flare observed on 1992 February 2.
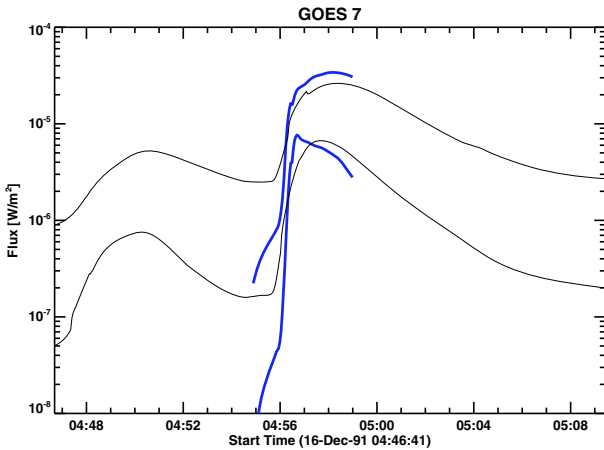

Fig. 3. Synthetic X-ray fluxes in 0.5–4 Å and 1–8 Å bands calculated using a numerical model of the M2.7 class solar flare observed on 1991 December 16 (blue thick line) and the corresponding fluxes recorded with the *GOES* 7 satellite (thin grey lines).

the energy used for the evaporation process while still fixing the total energy flux delivered by non-thermal electrons:

$$\Phi = \int_{E_c}^{\infty} A E^{-\delta} E \, \mathrm{d}E = \frac{A}{\delta - 2} E_c^{2-\delta}. \tag{2}$$

For each time step during each flare and with values of δ and E_c chosen such that Φ is a constant, one can calculate the appropriate value of A from Eq. (2). This allows one to generate a set of possible electron beams, all with identical total energy (integrated over the whole impulsive phase of the event) and identical time variations in the energy flux, and to use them to calculate a grid of models for each flare (see Fig. 4). For this work, we defined the impulsive phase of each flare to be the period when the hard X-ray flux recorded in the HXT/M1 channel was higher than 10 percent of the maximum flux.

We used a modified Naval Research Laboratory solar flux tube model code kindly made available to the solar community by Mariska and his co-workers (Mariska et al. 1982, 1989). Although a typical flaring loop is a 3-D structure surrounded by a possibly complex active region, it can be modeled for many purposes with both a simple 1-D hydrodynamic model and the NRL Code. We included a few modifications to the code: new radiative loss and heating functions; inclusion of the VAL-C model (Vernazza et al. 1981) of the initial structure of the lower part of the loop (extended using Solar Standard Model data; Bahcall & Pinsonneault 2004), and use of double precision in the calculations. The heating of the plasma by a non-thermal electron beam was modeled using the approximation given by Fisher (1989). A mesh of new values of the radiative loss function was calculated using the CHIANTI (version 5.2) software (Dere et al. 1997; Landi et al. 2006) for the temperature 10^4-10^8 K and densities range 10^8-10^{14} cm^{-3}. For each flare, a grid of models was calculated using various non-thermal electron beam models, all having the same total energy. All models were calculated for periods lasting from the beginning of the impulsive phase to beyond maximum of the soft X-ray emissions. These periods were about 150–200 s. The time steps in the models were about 0.0005–0.001 s.

We estimated the evaporation energy E_{evap} to be the difference between the total energy delivered by the non-thermal electrons E_{nth} and the total energy lost by radiation over the entire loop, E_{rad} (i.e. $E_{evap} = E_{nth} - E_{rad}$) during the impulsive phase. As mentioned before, the main parameters of each calculated model (time-dependent fluxes of the non-thermal electrons, and the lengths and cross-sections of the flaring loops) were evaluated using observational data (see Sect. 2).

energy distribution. A variation in the E_c value of just a few keV can add or remove a substantial amount of energy from/to the modeled system, so E_c must be selected with great care. We estimated E_c as follows. First, we derived low energy cut-offs of the energy spectra using the slightly modified semi-analytical model of McDonald et al. (1999). While these authors used a fixed value of E_c (equal to 20 keV) for all flares, we calculated E_c for each flare using an iterative method. The flare energy budget was calculated using *GOES* and HXT data. When the total energies calculated from HXR data and those emitted in the SXR range disagreed, we iteratively changed the value of E_c (in steps of 0.1 keV) until agreement was reached. This method is the most direct way of estimating E_c from the energy balance. We then slightly modified the value of E_c yet further to obtain the closest agreement between the synthesised and observed *GOES* classes and BCS fluxes of each flare. Examples of the agreement between observed and synthesised BCS light curves are shown in Fig. 2, while the observed and synthesised *GOES* curves are shown in Fig. 3. The estimated E_c was used as a fixed value, while the electron spectral index δ and corresponding scaling factor A varied in time for each particular model of event. The values of the main physical parameters, including γ and estimated E_c, observed at the maximum of the HXR emission, are given in Table 1 for all twelve flares.

By vary the electron energy spectral index δ and appropriate adjustment of A and E_c, one can easily change the amount of

Table 2. Results of the numerical models of analysed flares.

Event date	OBSERVATIONS GOES class*	MODEL			
		Minimum		Maximum	
		GOES class*	$E_{\rm evap}/E_{\rm nth}$	GOES class*	$E_{\rm evap}/E_{\rm nth}$
16-Dec.-91	M2.8 (M2.7)	C2.4 (C1.4)	0.07	M9.5 (M9.4)	0.79
02-Feb.-92	C5.5 (C2.7)	C3.4 (B6.3)	0.17	C8.4 (C5.6)	0.78
27-Oct.-92	M1.1 (C9.5)	C2.5 (B9.5)	0.08	M1.8 (M1.6)	0.82
03-Oct.-93	C1.0 (B8.1)	B6.5 (B4.4)	0.19	C2.8 (C2.6)	0.71
07-Mar.-93	C1.5 (B9.2)	B9.5 (B3.7)	0.07	C2.4 (C1.8)	0.70
26-Jan.-94	C1.4 (C1.1)	B7.4 (B4.4)	0.22	C2.8 (C2.5)	0.84
30-Jun.-99	M1.9 (M1.8)	C2.0 (B9.9)	0.04	X1.1 (X1.1)	0.71
22-Dec.-99	C6.4 (C5.4)	C2.1 (C1.1)	0.06	M4.5 (M4.4)	0.66
27-Jul.-00	M2.4 (M2.3)	C4.2 (C3.2)	0.11	M4.7 (M4.6)	0.80
06-Apr.-01	C7.8 (C4.9)	C4.5 (C1.5)	0.07	M3.1 (M2.8)	0.68
08-Sep.-01	C5.1 (C3.2)	C1.9 (A2.4)	0.02	M1.4 (M1.2)	0.51
18-Sep.-01	M1.5 (M1.3)	C3.1 (C1.1)	0.05	M4.8 (M4.6)	0.72

* *GOES* class minus the preflare level is given in parentheses.

4. Results

We analysed each flare in two steps. First, we compiled a model using observed geometrical and physical parameters, including δ and $E_{\rm c}$. The correctness of these models was validated by comparing the synthesised *GOES* 1–8 Å and 0.5–4 Å, BCS SXV and BCS CaXIX fluxes with the observed fluxes. We found good agreement between observations and the modeled data. For example, the observed and synthesised BCS SXV and BCS CaXIX fluxes of the C2.7 class solar flare observed on 1992 February 2 are shown in Fig. 2 while the calculated and observed *GOES* X-ray light-curves of the M2.7 event on 1991 December 16 are shown in Fig. 3. The values of the flux maxima are reproduced very well but the noticeably large discrepancies during the early rise and late decay phases are caused by a lack of additional pre- and post-impulsive flare heating in our model. In the second step, we calculated several numerical models of each event for various appropriate combinations of the electron spectral index δ and low-energy cut-off $E_{\rm c}$, where the total energy delivered by the non-thermal electrons was fixed to be equal to the observed energy.

The model calculations also provide e.g., pressure, temperature, density, velocity and column mass as functions of time and position along the loop. For all reasonable sets of physical parameters of the flaring loops, we found a rapid inflow of chromospheric material into the loop (i.e., chromospheric evaporation). Large-scale macroscopic motions of the dense plasma toward the loop-tops and rapid increases in the plasma temperature, pressure, and electron density all agree well with commonly accepted schemes of chromospheric evaporation. After the energy deposition period, the plasma contained in the flaring loop gradually cools, but the model calculations generally ended before returning to a hydrostatic equilibrium.

For all twelve flares, we found that by fixing the total energy delivered by non-thermal electrons, the resulting observed *GOES* class of the induced solar flare varied significantly when the spectral index and low energy cut-off of the non-thermal electrons spectra were changed. The variations in the *GOES* classes and the proportion of the total energy contributed by evaporation are given in Fig. 4. The upper-left panel shows models of M2.7 *GOES* class correlated flare observed on 1991 December 16. The observed low energy cut-off $E_{\rm c}$ is equal to 25.8 keV and is assumed to remain constant during the calculations. The spectral index δ is equal to 4.6 (here and for the

other three events shown in Fig. 4, we indicate the value of δ at the time of maximum of the impulsive phase). The upper-right panel shows models of the C2.7 *GOES* class non-correlated flare observed on 1992 February 2. The observed $E_{\rm c}$ and δ are equal to 18.9 keV and 4.0. The lower-left panel shows models of the B8.1 *GOES* class non-correlated flare observed on 1993 October 3. The observed $E_{\rm c}$ and δ are equal to 23 keV and 3.7, respectively. The bottom right panel shows models of the M2.4 *GOES* class correlated flare observed on 2000 July 27. The observed $E_{\rm c}$ and δ are equal to 19.8 keV and 4.2, respectively. The spectral indexes δ of each model varied in time while its observational values increased or decreased by a constant factor, i.e., in our models, we took various values of δ that differed from $\delta_{\rm obs}$ by between 0 and ± 2, where $\delta_{\rm obs}$ is the observed δ at any given time during the flare. The black, filled squares represent models calculated using non-thermal electron beams with main parameters that were deduced from observations. The total ranges of the modeled *GOES* classes and $E_{\rm evap}$ for all flares are shown in Table 2.

We now describe results obtained for the most representative events, two correlated flares (1991 December 16, 2000 July 27) and two non-correlated flares (1992 February 2 and 1993 October 3). All flares had a simple, single-loop structure. In the following, *GOES* classes are given with the pre-flare level subtracted.

4.1. M2.7 flare on 1991 December 16

The M2.7 flare at 04:54 UT on 1991 December 16 occurred in an active region NOAA 6961 (N04W45). The flare appeared in SXR as a single loop with semi-length 15 400 km (see Fig. 1). The impulsive HXR (>23 keV) occurred between 04:55:50 UT and 04:56:28 UT. The cross-section of the loop was estimated from HXR images to be $S = 3.9 \times 10^{17}$ cm^2.

A flare model was calculated using parameters of the photon spectra γ and scaling factors a_0 calculated as a function of time from hard X-ray fluxes observed in the HXT $M1$ and $M2$ channels, while $E_{\rm c}$ was estimated and fixed to be equal to 25.8 keV. The total non-thermal electron energy was estimated to be $E_{\rm nth} = 1.2 \times 10^{30}$ erg, while the evaporation energy was $E_{\rm evap} = 3.6 \times 10^{29}$ erg (=0.3 $E_{\rm nth}$). Alternative models were calculated for the same total energy $E_{\rm nth}$ but with δ changed from the initial value of 4.6 by ± 2 and with $E_{\rm c}$ changed from the initial value of $E_{\rm c}$ by ± 4 keV (see Fig. 4, top-left panel). For δ lowered by 2 and $E_{\rm c}$ raised by 4 keV, the evaporation energy decreased
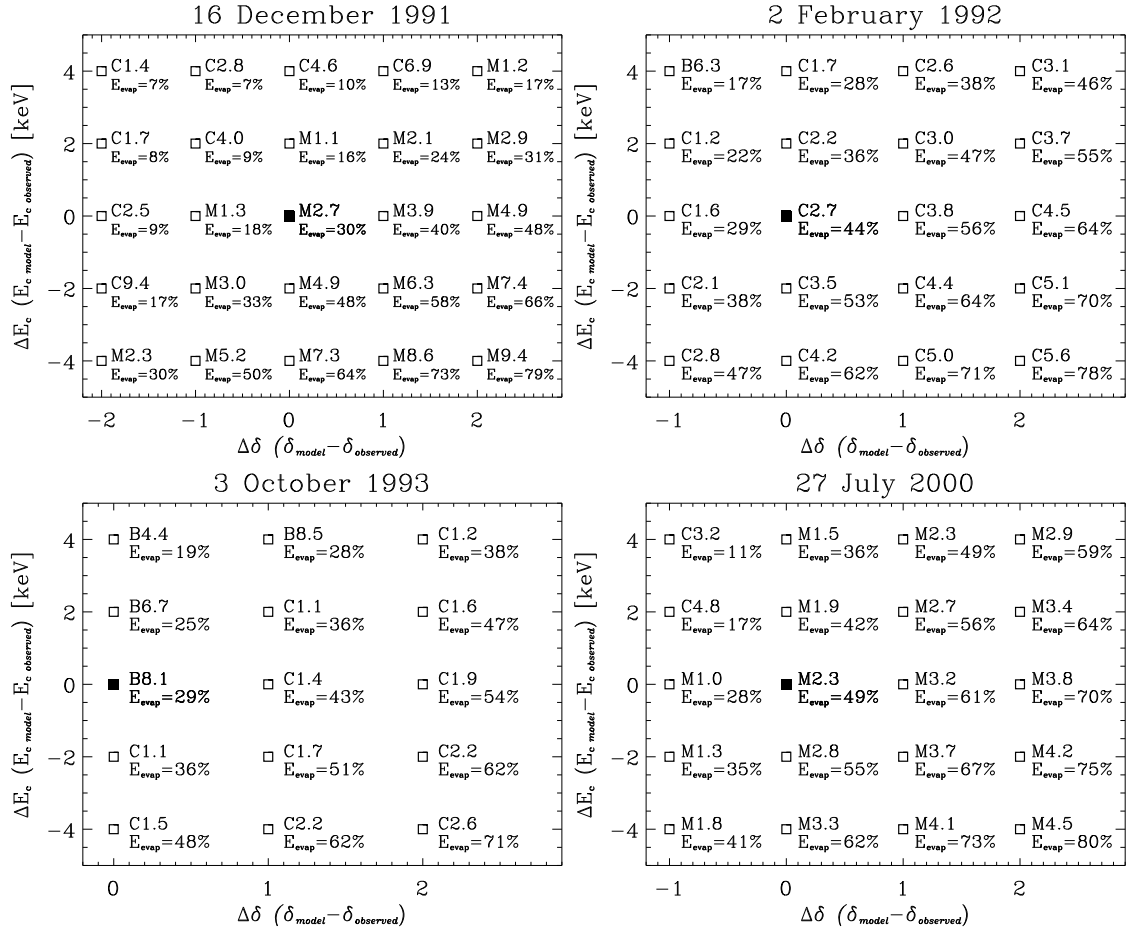
Fig. 4. Variations in the observed *GOES* classes and shares of the evaporation energy E_{evap} in the total energies delivered by non-thermal electrons for four solar flares observed on 1991 December 16, 1992 February 2, 1993 October 3 and on 2000 July 27. See Sect. 4 for details.

to 7% of E_{nth} only when the *GOES* class decreased to only C1.4. In contrast, when δ was increased by 2 and E_c lowered by 4 keV, the observed *GOES* class of the event increased to M9.4 while the evaporation energy increased to 79% of E_{nth}. Calculations made for all combinations of δ and E_c give flares of *GOES* class between C1.4 and M9.4.

4.2. C2.7 flare on 1992 February 2

The C2.7 flare on 1992 February 2 at 11:33 UT–11:38 UT occurred in the active region NOAA 7042 (S14W41). It was observed with HXT/*Yohkoh* and *GOES* only (see Fig. 1). The impulsive HXR (>23 keV) peak occurred between 11:33:18 UT and 11:33:28 UT, only 10 s long. HXT/LO images of the flare show the X-ray emission as a single loop of semi-length (≃9800 km). The loop foot points were observed only in HXT channels M2 and H. The loop cross-section was estimated to be $S = 2.3 \times 10^{17}$ cm^2.

The flare model was calculated as for the previous flare. The total energy was $E_{nth} = 1.7 \times 10^{29}$ erg and the evaporation energy was $E_{evap} = 7.5 \times 10^{28}$ erg, (=0.44E_{nth}). Alternative models were calculated for the same total non-thermal electron energy E_{nth} but with δ in the range -1 to $+2$ from the initial value of δ, and with E_c in the range ± 4 keV from the initial value of E_c (see Fig. 4, top-right panel). Calculations made for all combinations of spectral index and low energy cut-off give flares of *GOES* classes in the range B6.3 and C5.6.

4.3. B8.0 flare on 1993 October 3

The B8.1 flare on 1993 October 3 occurred between 09:06 UT and 09:07 UT in the active region NOAA 7590 (N11W04). The flare was visible in SXT as a single loop of semi-length ~28 800 km (see Fig. 1). The impulsive HXR (>23 keV) emission occurred between 09:06:40 UT and 09:07:15 UT. The cross-section of the loop was estimated to be $S = 1.4 \times 10^{17}$ cm^2.

A flare model was calculated using the total energy, which equaled $E_{nth} = 1.6 \times 10^{29}$ erg. The evaporation energy was equal to $E_{evap} = 4.6 \times 10^{28}$ erg, (=0.29E_{nth}). Alternative models were calculated for the same total energy E_{nth} but with δ changed by between 0 and $+2$ from the initial value of δ and with E_c changed from the initial value of E_c by ± 4 keV (see Fig. 4, bottom-left panel). The spectral index was increased by 2 and the energy cut-off was lowered by 2 keV, and the corresponding evaporation energy of the flare increased to 0.71 E_{nth} and the *GOES* class of the flare increased to C2.6. Calculations for all combinations of spectral index and energy cut-off provided flares of *GOES* classes varying from B4.4 to C2.6.

4.4. M2.4 flare on 2000 July 27

The M2.4 flare on 2000 July 27 occurred between 04:08 UT–04:13 UT in the active region NOAA 9090 (N10W72). The flare was visible in SXT as a single loop with semi-length ~8700 km (see Fig. 1). The HXR (>23 keV) emission occurred between 04:07:54 UT and 04:08:30 UT. Using the reconstructed HXR

images, we estimated the cross-section of the loop to be $S = 2.3 \times 10^{17}$ cm^2.

The flare model was calculated in the same way as for the previous events. The total energy was $E_{nth} = 4.8 \times 10^{29}$ ergs and the evaporation energy $E_{evap} = 2.3 \times 10^{29}$ ergs ($=0.44 E_{nth}$). The alternative models of the flare were calculated for the same total energy E_{nth} but by δ changing from its initial value by -1 to -2 and with E_c changed from the initial value of E_c by ± 4 keV (see Fig. 4, bottom-right panel). When the spectral index was increased by 2 and the energy cut-off lowered by 4 keV, the evaporation energy of the flare increased to 80% of E_{nth} and the *GOES* class of the flare increased to M4.5. In contrast, when δ decreased by 1 and E_c increased by 4 keV the observed *GOES* class of the event decreased to only C3.2, while the evaporation energy decreased to $0.11 E_{nth}$. Calculations for all combinations of δ and E_c produced flares with *GOES* classes varying from C3.2 to M4.6.

5. Discussion and conclusions

We have presented results of an energy model calculation for twelve flares with various soft to hard X-ray emission ratios. We focused on the influence of varying the energy spectrum of the non-thermal electrons on both the observed *GOES* classes of the flares and their evaporation energies E_{evap}. Many numerical models of the events were calculated using observed and modified energy distributions of the non-thermal electrons (various appropriate combinations of the electron spectral index δ and low energy cut-off E_c, but fixed values of the total energy delivered by non-thermal electrons E_{nth}), observed geometry of the loops, and initial values of the main physical parameters of the plasma estimated using observational data. We first showed that for fixed initial parameters of the flare loop (geometry and physical parameters of the plasma) and fixed total non-thermal electron energy, one can significantly change the resulting *GOES* class of the flare by appropriately changing of the electron index and low energy cut-off of the electron spectra while maintaining the total energy at a constant value. For example, we were able to convert the M2.7 *GOES* class correlated flare into a C1.4 class non-correlated-like flare, and a B8.1 *GOES* class non-correlated flare into a C2.6 class correlated-like flare.

The ratio of the radiated energy to the energy in evaporation processes, as well as the observed *GOES* classes of the events vary for various combinations of the spectral index and low energy cut-off. It is obvious that both the total delivered energy and the energy spectrum of the non-thermal electron beam (described by spectral index and low energy cut-off) are important to determining the course and magnitude of the evaporation processes and the observed soft X-ray emission of the flares (i.e., their *GOES* class).

An estimation of the energy carried by non-thermal electrons is very sensitive to an assumed value of the low energy cut-off of the energy spectrum due to the power-law nature of the energy distribution. A change in the E_c value of only a few keV can add or remove a substantial amount of energy from/to the modeled system. The spectral index of the non-thermal electron spectrum is also crucial, while the low-energy fraction of the electrons heats the chromospheres most effectively (see also McDonald et al. 1999). For the same total energy, the beam of non-thermal electrons with a softer spectrum could produce a solar flare of greater *GOES* importance. This is demonstrated in Fig. 4, where variations in the observed *GOES* classes and evaporation energies E_{evap} are shown for four flares. As an example, one can track the behaviour of the M2.7 flare on 1991 December 16. The

model calculated using a non-thermal electron beam with principal parameters deduced from observations, the *GOES* class is equal to M2.7 and the evaporation energy equals 30% of the total energy delivered by the non-thermal electrons. The same observed solar flare, modeled using a non-thermal electron beam of spectral index δ that has decreased by 1, has a slightly lower *GOES* class equal to M1.3 and significantly lower evaporation energy equal to 18% E_{nth}. By increasing additionally the low energy cut-off E_c by 2 keV, we obtained an even lower *GOES* class and E_{evap} model equal to C4.0 and 9% E_{nth}, respectively. In contrast, for a steeper electron spectrum and increased population of low energy electrons (decreased E_c), both the *GOES* classes and E_{evap} increase. Thus, for the M2.7 flare described above, the non-thermal electron beam that has an energy spectral index δ that has increased by 1, has a slightly higher *GOES* class of M3.9 and higher evaporation energy of 40% E_{nth}. By decreasing additionally the low energy cut-off E_c by 2 keV (and hence expanding the low-energy electron population), we obtained an even higher *GOES* class and E_{evap} of the model of M6.3 and 58%, respectively. The ranges of the modeled *GOES* classes and E_{evap} for all analysed events are given in Table 2.

The overall changes in *GOES* classes and E_{evap} are similar for all our analysed events. In general, the SXR emission increases for softer HXR spectra and decreases for harder spectra. That is, the steeper electron spectra produce a higher amount of evaporated material. This behaviour is induced by spatial variations in the efficiency of the non-thermal electron energy deposition mechanism. The energy deposition mechanism is most efficient in the transition region and upper part of the chromosphere, but its particular spatial distribution depends on the true distribution of the column mass of plasma encountered by non-thermal electrons. However, the magnitude of changes observed for a particular flare depends on the flare's physical properties.

A non-thermal electron beam containing a large population of high-energy electrons (i.e., with a hard spectrum) penetrates deep into the chromospheric plasma, where it deposits most of its energy, and from where energy is efficiently radiated. The remaining part of the transmitted energy is deposited in the upper part of the chromosphere and/or transition region, causing moderate "gentle evaporation". On the other hand, a non-thermal electron beam with a soft spectrum deposits most of its energy in the upper part of the chromosphere and/or transition region, where the density is relatively low, giving rise to "explosive evaporation".

Our results show that the parameters and properties of the solar flares depend not only on the initial hydrodynamic properties of the flaring loop and the total amount of the delivered energy but also on properties of the primary source of energy, and time and spatial variations in the processes leading to the electron acceleration. Thus, the level of correlation between the cumulative time integral of HXR and SXR fluxes depends on the HXR energy range. This conclusion is in accordance with results of the statistical analysis of flares by Veronig et al. (2002) and microflares by Qiu et al. (2004) observed with RHESSI indicating that only half of the events show a time behaviour consistent with the expectations based on the Neupert effect. Qiu et al. (2004) also showed that the correlation predicted by the Neupert effect is greatest for the photon energy range of 14–20 keV.

In Fig. 5, we show the variations in the synthesised *GOES* classes and X-ray fluxes of the numerical models of the four solar flares obtained for various E_c and δ and constant total energy delivered by non-thermal electrons. The arrows indicate the variations in the *GOES* classes and X-ray fluxes of the models, while the open circles represent 369 flares taken from the HXT
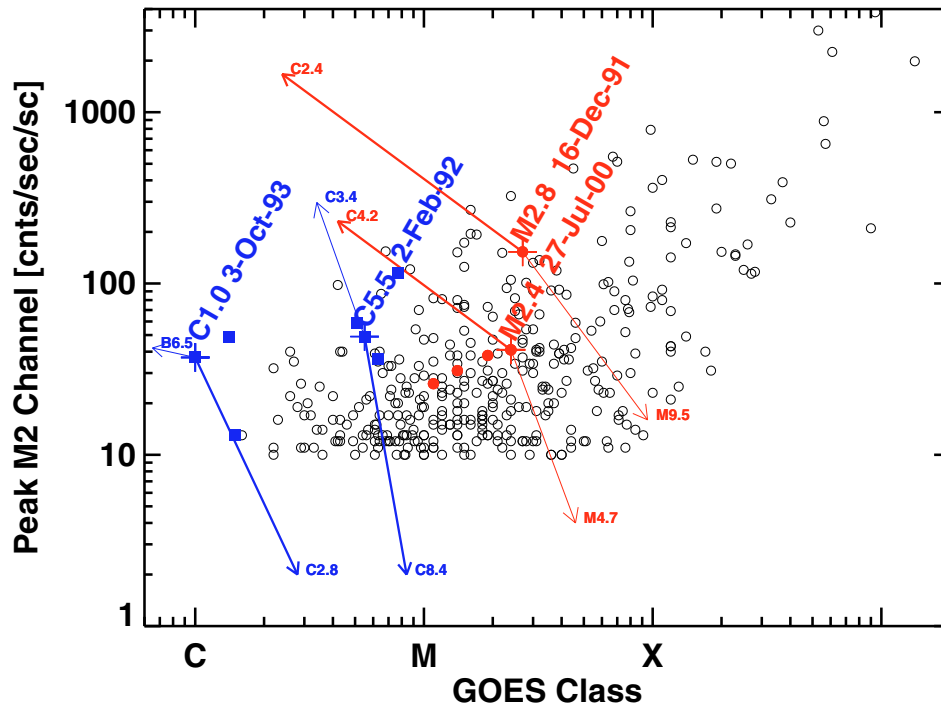
Fig. 5. Variations in the synthesised *GOES* classes and X-ray fluxes of the numerical models of the four solar flares obtained for various E_c and δ and constant total energy delivered by non-thermal electrons (see main text and Fig. 4 for details). The models calculated using observed energy spectra of non-thermal electrons are marked with crosses. The arrows show the variations in the *GOES* classes and X-ray fluxes of the models, the open circles representing 369 flares taken from the Sato HXT Flare Catalogue. Filled circles (red colour) denote five correlated and filled squares (blue colour) seven non-correlated analysed flares.

Flare Catalogue (Sato et al. 2006). As can be seen the, relationships between the soft and hard X-ray fluxes obtained from the models go far beyond the range of the "correlation belt" of soft and hard X-ray fluxes recorded for the observed solar flares, up to high HXR fluxes. For example, by changing the hardness of the non-thermal electron spectrum and low energy cut-off, the M2.7 flare observed on 1991 December 16 was converted into the C2.4 *GOES* class event with an HXT/M2 peak emission above 1000 cnts/s/sc (see Fig. 5, thick arrow). Many flares of low GOES class but high hard X-ray flux have been observed with *Yohkoh* and *RHESSI*. However, one does not appear observe flares of similar GOES class with high X-ray flux; these extremely "small-hard" flares do not appear to exist (i.e., flare that would be located in the upper-left corner at the Fig. 5). This than imposes restrictions on the flare electron spectra and therefore on acceleration mechanisms.

References

Bahcall, J. N., & Pinsonneault, H. M. 2004, Phys. Rev. Lett., 92, 12
Battaglia, M., Grigis, P. C., & Benz, A. O. 2005, A&A, 439, 737

Brown, J. C. 1971, Sol. Phys., 18, 489
Brown J. C., Emslie, A. G., Holman, G. D., et al. 2006, ApJ, 643, 523
Culhane, J. L., Bentley, R. D., Hiei, E., et al. 1991, Sol. Phys., 136, 89
Dennis, B. R., & Zarro, D. M. 1993, Sol. Phys., 146, 177
Dere, K. P., Landi, E., Mason, H. E., Monsignori-Fossi, B. C., & Young, P. R. 1997, A&AS, 125, 149
Gburek, S., & Siarkowski, M. 2002, Adv. Space Res., 30/3, 601
Hannah, I. G., Christe, S., Krucker, S., et al. 2008, ApJ, 677, 704
Fisher, G. H. 1989, ApJ, 346, 1019
Kontar, E. P., Dickson, E., & Kaparov, J. 2008, Sol. Phys., 252, 139
Kosugi, T., Masuda, S., Makishima, K., et al. 1991, Sol. Phys., 136, 17
Lin, R. P., Schwartz, R. A., Kane, S. R., et al. 1984, ApJ, 283, 421
Landi, E., Del Zanna, G.,Young, P. R., et al. 2006, ApJS, 162, 261
Mariska, J. T., Boris, J. P., Oran, E. S., Young, T. R. Jr., & Doschek, G. A. 1982, ApJ, 255, 738
Mariska, J. T., Emslie, A. G., & Li, P. 1989, ApJ, 341, 1067
McDonald, L., Harra-Murnion, L. K., & Culhane, J. L. 1999, Sol. Phys., 185, 323
Metcalf, T. R., Hudson, H. S., Kosugi, T., Puetter, R. C., & Pina, R. K. 1996, ApJ, 466, 585
Neupert, W. M. 1986, ApJ, 153, L59
Qiu, J., Liu, C., Gary, D. E., Nita, G. M., & Wang, H. 2004, ApJ, 612, 530
Sato, J., Matsumoto, Y., Yoshimura, K., et al. 2006, Sol. Phys., 236, 351
Siarkowski, M., Falewicz R., & Berlicki A. 2006, Adv. Space Res., 38/5, 972
Siarkowski, M., Falewicz, R., Kepa, A., & Rudawy, P. 2008, Ann. Geophys., 26, 2999
Tandberg-Hanssen, E., & Emslie, A. G. 1988, The physics of solar flares (Cambridge University Press)
Thomas, R. J., Crannell, C. J., & Starr, R. 1985, Sol. Phys., 95, 323
Tsuneta, S., Acton, L., Bruner, M., et al. 1991, Sol. Phys., 136, 37
Vernazza, J., Avrett, E., & Loeser, R. 1981, ApJS, 45, 635
Veronig, A., Vrsnak, B., Dennis, B. R., et al. 2002, A&A, 392, 699
White, S., Thomas, R. J., & Schwartz, R. A. 2005, Sol. Phys., 227, 231